Short activation domains control chromatin association of transcription factors

Vinson B Fan[1], Xavier Darzacq[1], Max V Staller[1, 2, 3]

[1] Department of Molecular and Cell Biology, University of California Berkeley, Berkeley, 94720
[2] Center for Computational Biology, University of California Berkeley, Berkeley, 94720
[3] Chan Zuckerberg Biohub–San Francisco, San Francisco, CA 94158

Abstract

Transcription factors regulate gene expression with DNA-binding domains (DBDs) and activation domains. It is generally assumed that DBDs are solely responsible for interacting with DNA and chromatin. Here, we used single-molecule tracking of transcription factors in living cells to find that short activation domains can control the fraction of molecules bound to chromatin. Activation domains with high bound fractions also have longer residence times on chromatin. Mutations in activation domains that increase activity of a transcriptional reporter increase the fraction of molecules bound to chromatin. Reciprocally, mutations that decrease reporter activity decrease fraction bound. These effects were consistent across three activation domains and three DBD classes. Taken together, these results suggest that activation domains play a major role in tethering transcription factors to chromatin, challenging the traditional view that the DBD is solely responsible for binding chromatin.

Introduction

Transcription factors (TFs) are classically described as modular proteins containing two parts: DNA-binding domains (DBDs) that bind cognate DNA motifs and independently-acting effector domains that regulate transcription (Brent and Ptashne, 1985). DBDs are ordered, conserved, and readily predicted from protein sequences (El-Gebali et al., 2019; Finn et al., 2016). Outside the DBD, TFs are predominantly composed of long intrinsically disordered regions (IDRs) that contain short repression domains, which bind corepressor complexes, and activation domains, which bind coactivators. Activation domains recruit remodelers, like BAF, that move nucleosomes, coactivators, like p300/CBP, that modify chromatin, and/or the basal transcriptional machinery that recruits RNA polymerase II (Alerasool et al., 2022; Gill et al., 1994). Although mechanistic understanding of activation domains still lags far behind DBDs, recent screens have cataloged many activation domains, and predictive models are improving (DelRosso et al., 2023; Erijman et al., 2020; Kotha and Staller, 2023; Morffy et al., 2024; Sanborn et al., 2021). The function of acidic activation domains, the oldest and largest class, depends on a balance of acidic, aromatic, and leucine residues (Staller et al., 2022, 2018; Udupa et al., 2024). For consistency, in this work we define activation domain strength as the fluorescence of a GFP reporter construct.

TFs can bind DNA, and they can bind chromatin. For this paper, it is important to distinguish between DNA binding and chromatin binding. DNA binding results from direct protein-DNA interactions and is well established for DBDs *in vitro* (Stormo, 2013). Chromatin binding includes DNA binding but can also result from protein-protein interactions with histones or other DNA-bound proteins, including other TFs, corepressors, and coactivators. Nearly all cell-based assays of TF genome localization (e.g. ChIP-seq) measure the combination of DNA binding and chromatin binding.

In the traditional model of TF function, the DBD scans the DNA and binds to a cognate motif, and only then does the activation domain recruit coactivators from solution (Brent and Ptashne, 1985). In this model, activation domains do not contribute to genomic localization, DNA binding, or chromatin binding. This model further predicts that two TFs with different activation domains but the same DBD will have indistinguishable DNA binding and chromatin binding.

Recent data challenge the strictest form of this traditional model. *In vitro*, intramolecular interactions in p53 between the activation domain and DBD increase DNA specificity (Ning et al., 2022; Sun et al., 2021). A single-molecule footprinting (SMF) assay found that a strong activation domain can increase TF occupancy in a

feedforward manner dependent on the nucleosome remodeler BAF (Doughty et al., 2024). We have previously shown that long IDRs control the fraction of TF molecules bound to chromatin for factors in the HIF family (Chen et al., 2022). Finally, there is extensive literature demonstrating how long IDRs of TFs can control TF genomic localization (Brodsky et al., 2020; Gera et al., 2022; Mindel et al., 2024a). These authors show that long IDRs are necessary and sufficient to localize TFs to target promoter genes and that minimal activation domains are neither necessary nor sufficient for this genomic localization (Brodsky et al., 2020; Gera et al., 2022; Mindel et al., 2024a)). This result was interpreted as directed DNA binding by IDRs, but the existing data cannot distinguish between direct DNA binding and chromatin binding via protein-protein interactions with DNA-bound factors.

These studies demonstrate how long IDRs modulate or dominate functions ascribed to the DBD. In this study, we asked if short activation domains within an IDR are sufficient to control chromatin association.

We find that short activation domains are sufficient to control the fraction of molecules bound to chromatin. We use single-molecule tracking (SMT) to quantify the fraction of molecules bound to chromatin and fluorescence recovery after photobleaching (FRAP) as a proxy for TF residence time on chromatin. Activation domains consisting of 39-46 amino acids (AAs) can control the fraction of molecules bound to chromatin. Strikingly, mutations that increase activation domain strength increase the fraction of TF molecules bound to chromatin and increase residence times on chromatin. This effect was observed with activation domains attached to three structurally diverse DBDs, indicating that activation domains can control TF association with chromatin independent of DBD identity. These results suggest a key aspect of activation domain function could derive from increasing the ability of a TF to interact with chromatin productively.

Results

Single-molecule tracking of a synthetic transcription factor

To test whether short activation domains are sufficient to control chromatin binding of transcription factors, we performed SMT on a synthetic transcription factor. This synthetic TF was developed for high-throughput reporter studies of activation domain function (Staller et al., 2022) and contains an estrogen-binding domain for inducible activation and six synthetic C2H2 zinc fingers (Park et al., 2019) engineered to bind to a DNA motif that is not found in human cells. We added a HaloTag for labeling with photostable synthetic dyes (Grimm et al., 2021) to facilitate SMT (Fig. 1A). Candidate activation domains and their rationally-designed mutants were fused to the N-terminus of this chassis. We also engineered the cognate reporter into the AAVS1 locus of U2OS cells and derived a monoclonal line to assay transcriptional activity by GFP expression (Fig. 1B, Methods). For the synthetic DBD, our reporter locus is the only perfect motif match in the genome. We stably integrated each synthetic transcription factor into this cell line and verified that estradiol induction robustly induces GFP expression (Fig. 1C).

We performed SMT on these synthetic TFs using highly inclined and laminated optical sheet (HILO) illumination at fast (7.5 ms) frame rates (Fig. 1D). After extracting trajectories from movies, we used a published Bayesian mixture model to recover diffusive states from within these trajectories (Heckert et al., 2022). This approach to analyzing the SMT data generates a distribution of diffusion rates for each synthetic TF. With sufficient trajectories, these spectra are interpreted as steady-state probabilities of the TFs occupying different diffusion coefficients. We define proteins with a diffusion coefficient $D < 0.1\ \mu m^2/s$ as immobile and assume immobile molecules are bound to chromatin (Chen et al., 2022; Ferrie et al., 2024). Importantly, this chromatin association does not necessarily indicate direct binding to DNA but could include interactions with factors directly bound to DNA. Molecules with higher diffusion coefficients are considered untethered and are likely freely diffusing or complexed with other factors. In this work, we focus on the fraction of immobile molecules bound to chromatin.

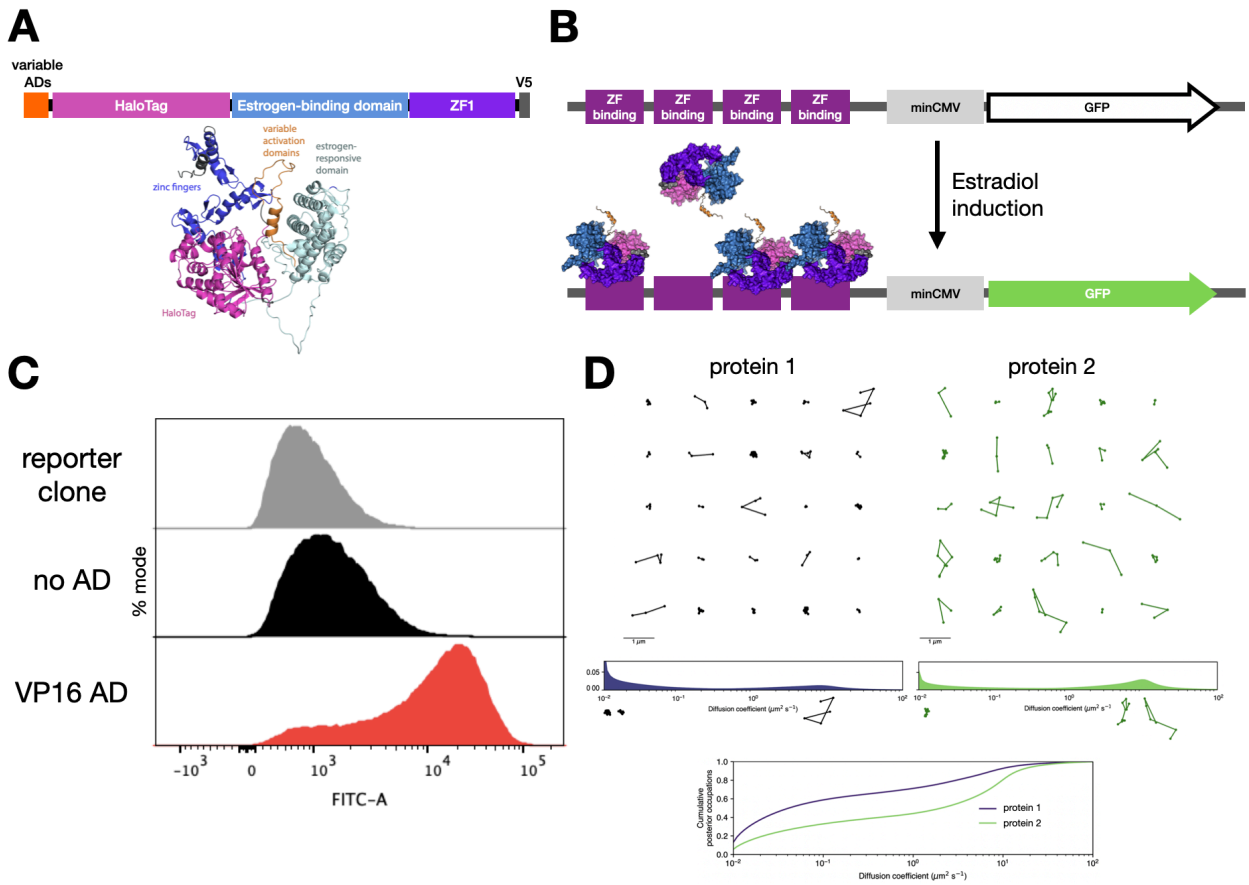

Figure 1: A synthetic transcription factor for quantification of fraction of molecules bound to chromatin

A: Schematic and AlphaFold2 model of a synthetic transcription factor. Activation domains (39-46 AA) are fused to HaloTag, an estrogen-binding domain, six synthetic C2H2 zinc fingers, and V5 epitope tag. Black regions indicate linkers between functional domains.

B: Schematic of the AAVS1 reporter locus (not to scale). Four zinc-finger binding sites are engineered upstream of a minimal promoter (minCMV) driving GFP.

C: Flow cytometry measurement of reporter induction after twenty-eight hours of estradiol treatment. Reporter clone: parental cell line from which other cell lines were derived (Methods), no AD: synthetic transcription factor shown above with no activation domain, VP16: 39 amino acids from VP16 H1 fused to the synthetic TF.

D: Trajectories extracted from SMT movies from two proteins. Thousands of trajectories are pooled to generate inferred diffusion spectra. Lower panel indicates the cumulative density function of the diffusion spectra.

Short activation domains control the fraction of TF molecules bound to chromatin

Given the evidence that long IDRs can control the fraction of molecules bound to chromatin, we tested the hypothesis that minimal activation domains can also contribute to this phenotype. In previous examples, the IDRs that controlled the bound fraction were the majority of the protein (Chen et al., 2022). Here, our synthetic TF is ~800 AAs and the activation domain is 39-46 (~5%) residues on the N-terminus.

We found that the short activation domains tested dominate the bound fraction of our synthetic TF. Three acidic activation domains derived from VP16, CITED2, and HIF1α each yielded different bound fractions and diffusion spectra (Fig. 2A). These differences are apparent in jump-length histograms and generally agree with parameters modeled from Spot-On (Hansen et al., 2018; Fig. S1), validating our Bayesian inference scheme. This bound fraction is positively correlated with GFP expression of the reporter locus measured by flow cytometry (Fig. 2B, C) and suggests a link between the strength of activation domains and their propensity to associate with chromatin. The synthetic TF without an activation domain also had a low fraction of molecules bound to chromatin.

As previously reported (Driouchi et al., 2023; Walther et al., 2024), we find substantial cell-to-cell variance when making SMT measurements in these cell lines (Fig. S2), which necessitated large datasets with many cells and trajectories for reporting reproducible diffusion spectra (Methods). The difference in bound fractions also holds when these synthetic TFs are transfected into cells without reporter loci (Fig. S3). This result strongly suggests that the majority of immobile particles are binding nonspecifically to genomic sites without a match to the cognate motif.

To complement the SMT, we measured TF residence time on chromatin with fluorescence recovery after photobleaching (FRAP). SMT at fast frame rates provides snapshots of the diffusive states of these factors but cannot accurately determine how long a given factor remains bound. The high laser power needed for SMT causes significant photobleaching, which obscures the dwell times of immobile molecules. To assay TF residence time on chromatin, we used FRAP for two of these synthetic factors (Fig. 2D, S4). We found that SMT bound fraction correlated with FRAP recovery times, with stronger activation domains conferring longer dwell times. This recovery time difference is consistent with other synthetic systems (Trojanowski et al., 2022). Together, these results indicate that stronger activation domains have a high fraction of molecules bound to chromatin, and these molecules have longer residence times on chromatin.

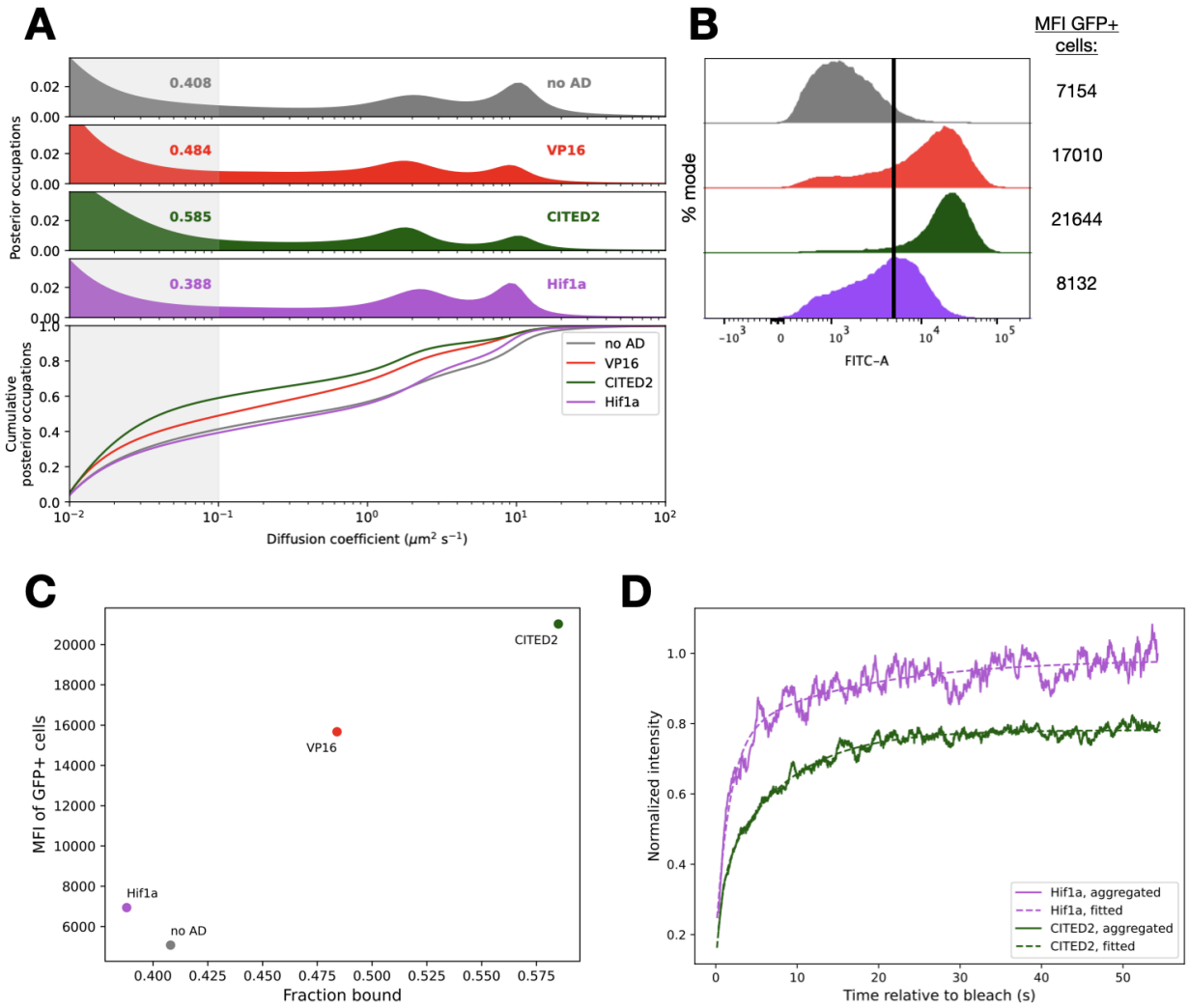

Figure 2: Short activation domains are sufficient to control the fraction of TF molecules bound to chromatin

A: Diffusion spectra of synthetic TFs bearing various activation domains (top) and cumulative distributions (bottom). Numbers indicate the fraction of molecules below a cutoff of 0.1 μm2/s, which we consider to be immoble and infer to be bound to chromatin.

B: Reporter activity of cells bearing these activation domain TF constructs after 28 hours of estradiol induction, as measured by flow cytometry. The black line is the gate for GFP+ cells. MFI is the geometric mean of GFP values for cells in the positive gate.

C: For each synthetic TF, the mean fluorescence intensity of GFP+ cells is plotted against the bound fraction.

D: HIF1α and CITED2 aggregated FRAP recoveries plotted as rolling means (solid lines), including curve fits to a double-exponential equation (dashed lines).

Mutations in individual activation domains change chromatin binding

Intrigued by the apparent correlation between activation domain strength and bound fraction, we next investigated multiple allelic series of mutations that increased and decreased activity of our activation domains (Staller et al., 2022). We selected mutants that we have previously shown to have large effects on reporter gene activity and that change 1-7 residues in each activation domain.

Within each allelic series, we saw a correlation between activation domain strength and bound fraction. These mutations change activity by perturbing different physicochemical parameters. For CITED2 (Fig. 3A), two alleles that decrease activity, either by mutating key hydrophobic residues (motif mutation) or replacing all six leucines with phenylalanines (L>F), decreased bound fraction. A CITED allele that neutralizes a single positive charge (K>A) increased activity and increased bound fraction. For VP16, we imaged two alleles that abrogate activation domain activity, F442A (Cress and Triezenberg, 1991) and 7As, and found both reduced the bound fraction (Fig. 3B). In HIF1α, adding acidity by mutating three arginines to aspartates (R>K) or two glutamines and one asparagine to glutamate (QN>E) increased the fraction bound (Fig. 3C). We employed a bootstrapping approach to estimate error in SMT diffusion spectra (Methods, Fig. S5) and present a summary of our measurements in Fig. 3D. Overall, stronger activation domain mutants had higher bound fractions, and weaker mutants had lower bound fractions. This trend holds within each allelic series and across the full set of mutants.

Furthermore, for HIF1α, the QN>E allele has slower FRAP recovery, indicating a longer residence time on chromatin (Fig. S6D). These data suggest that strong activation domains increase the fraction of TF molecules bound to chromatin and extend their duration of binding.

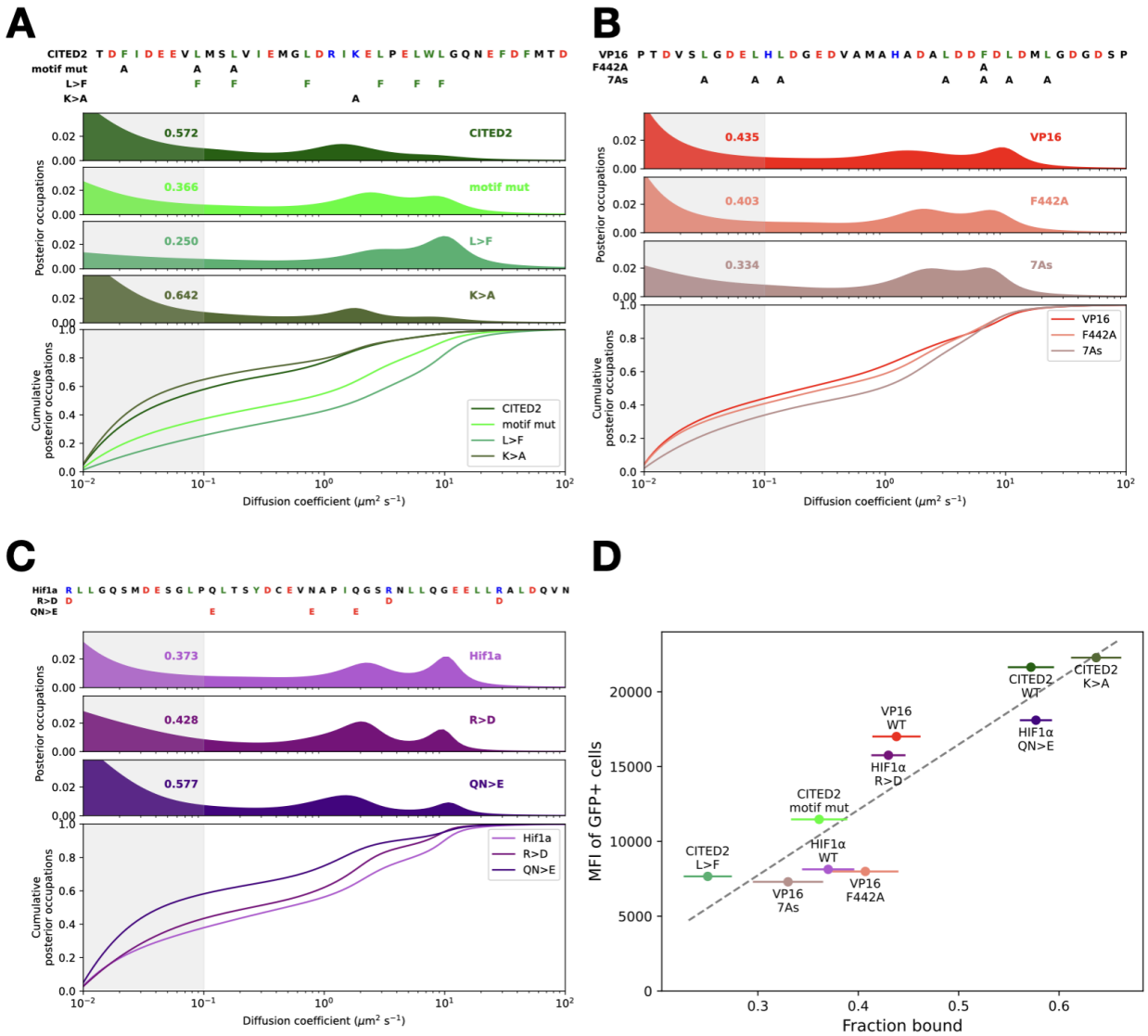

Figure 3: Mutations in individual activation domains change the fraction of molecules bound to chromatin

A: For CITED2, the amino-acid sequence of the WT and mutant constructs is shown above the diffusion spectra and the cumulative density functions. The fraction of bound molecules (immobile fraction) is quantified.

B: as in A for VP16.

C: as in A for HIF1α.

D: Summary of activation domain activity and bound fractions. Mean fluorescence intensity of GFP+ cells plotted against bound fractions. Error bars indicate standard deviations of a cell-wise bootstrapping scheme (Methods, Fig. S5).

Activation domains control chromatin binding of a second DBD

We next tested whether the observed relationship between activation domain strength and bound fraction depends on the DBD of our synthetic factor. To do this, we replaced the synthetic zinc fingers with the SOX2 DBD, which belongs to a different family of DBDs, the high-mobility group (HMG) family. These domains are minor-groove binders with many specific cognate sites throughout the genome. For this orthogonal DBD, our CITED2-K>A mutant had a dramatically higher fraction bound than WT, while the inactive motif mutant modestly decreased chromatin association (Fig. 4A). The L>F mutation in this chimeric factor prevented its localization to the nucleus, precluding SMT. None of these constructs activated our GFP reporter, validating that cognate-site binding is required for the activation of the reporter locus (Fig. S8). This last finding further suggests that most of the observed chromatin binding is not at the reporter locus.

Activation domains control chromatin binding of full length TFs

We next investigated activation domain mutations in full length TFs. We previously showed that the bound fraction of the HIF1α and HIF2α paralogs are controlled by long IDRs, not their DBDs (Chen et al., 2022). In chimeric TFs, the IDR determines the bound fraction, with HIF2α's IDR leading to more association with chromatin and HIF1α's with less chromatin binding. Previous studies were conducted in VHL-deficient renal carcinoma cells, which resulted in the stabilization of HIF proteins in this cell line (Brodaczewska et al., 2016). We recapitulated these results in our U2OS cells using desferrioxamine, a drug that prevents HIF degradation and mimics aspects of hypoxia (Guo et al., 2006). In this condition, we reproduced the effect of IDR swaps on the diffusion of HIF factors: HIF2α had a higher bound fraction than HIF1α, and the HIF2α IDR was sufficient to confer this higher bound fraction (Fig. 4B). Conversely, the HIF1α IDR conferred a lower bound fraction when attached to the HIF2α DBD. For these paralogs, the IDR controls the bound fraction.

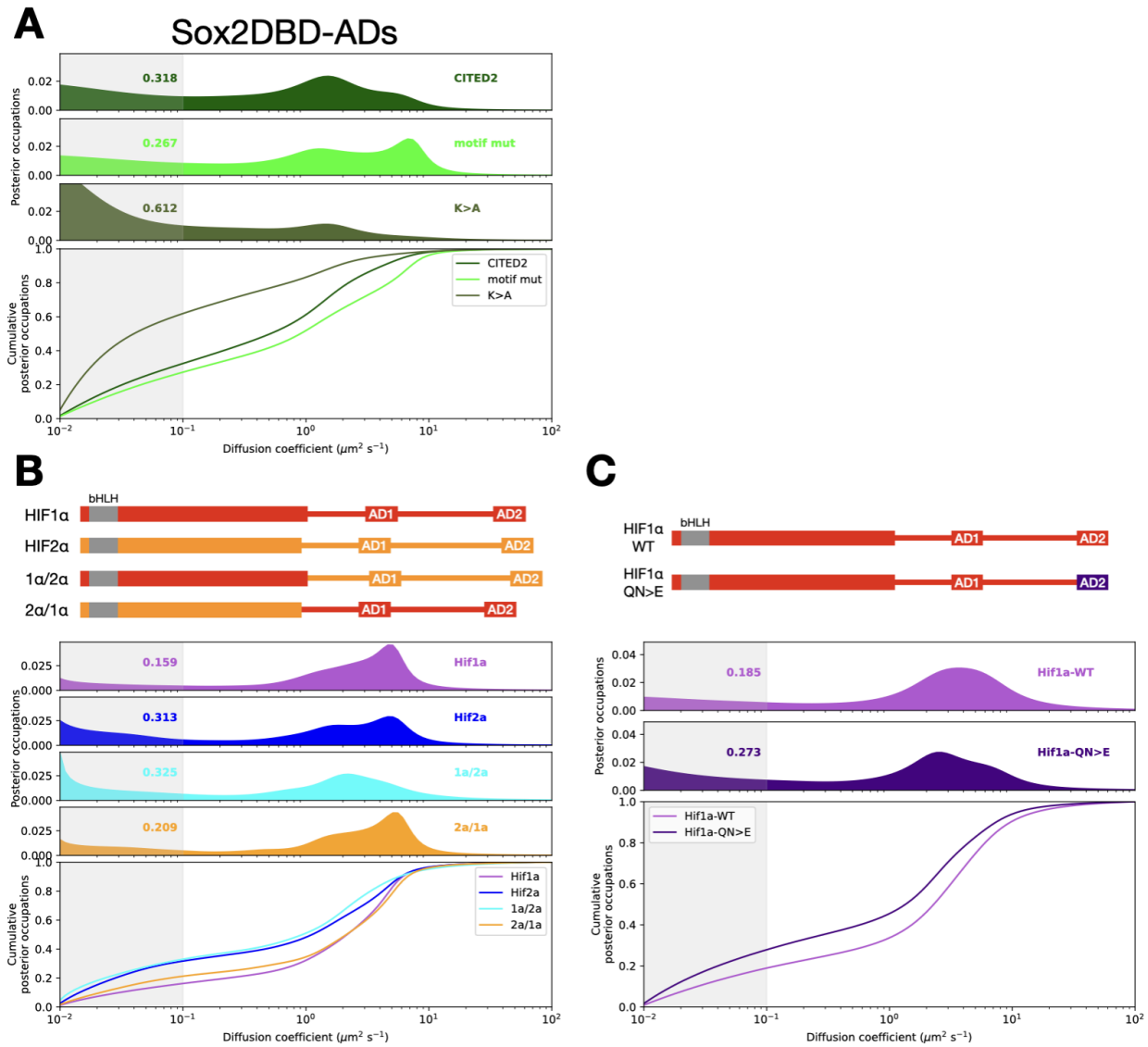

Figure 4: Activation domain alleles control the fraction of molecules bound to chromatin when fused to an alternative DBD or in a full length TF

A: We replaced the synthetic zinc finger DBD with the hSox2DBD and imaged three CITED2 alleles.

B: Top: Schematic of the HIF1α and HIF2α IDR swap chimeras from (Chen et al., 2022). The DBD (bHLH) and two activation domains are shown. Bottom: the HIF1α IDRs control the fraction of molecules bound to chromatin under hypoxic conditions.

D: Schematic of three point mutations in the second HIF1α activation domain.

E: These HIF mutations change the fraction of molecules bound to chromatin, recapitulating the differences seen in synthetic TFs.

We tested if the mutations in the activation domain could control the fraction of full-length HIF1α bound to chromatin. We introduced the strongest of these mutations, QN>E, into AD2 (C-AD) of full-length HIF1α. We found that this mutant activation domain increased the fraction of molecules bound to chromatin (Fig. 4C). This result shows that the strength of activation domains in endogenous factors can control the fraction of molecules bound to chromatin. This finding opens the door to a new dimension of activation domain function: increasing chromatin binding. Further, this experiment demonstrated that the relationship between activation domain strength and bound fraction holds for another structurally distinct DBD, the basic helix-loop-helix (bHLH) family.

Together, we found that strong activation domains can modulate the bound fraction of one synthetic and two natural DBDs. These DBDs are taken from three structurally distinct classes: zinc finger, HMG, and bHLH. We have further shown this result holds for both synthetic TFs and endogenous TFs. We speculate that acidic activation domains may contribute to the fraction of molecules bound to chromatin for other full length TFs.

Disrupting coactivator function perturbs TF-chromatin associations

We explored the hypothesis that protein-protein interactions between activation domains and coactivators can explain the observed relationship between activation domain strength and the fraction of molecules bound to chromatin. If increasing activation domain binding to known coactivator partners can increase TF chromatin binding, it would explain our results without invoking any new molecular interactions. *In vitro*, strong activation domains bind coactivators more tightly than weak ones (DelRosso et al., 2024; Henderson et al., 2018; Sanborn et al., 2021). In the nucleus, coactivators are limiting for transcriptional activity (Gillespie et al., 2020). The coactivator p300 has a high bound fraction and relatively long residence time (Ferrie et al., 2024) and it is a key binding partner for the HIF1α, CITED2, and VP16 activation domains. We set out to investigate the hypothesis that activation domain binding to coactivators can tether TFs to chromatin by pharmacologically perturbing coactivator function.

Inhibition of p300 with A485 increases the fraction of p300 molecules bound to chromatin (Ferrie et al., 2024). A485 inhibits p300 catalytic activity and decreases global transcription (Lasko et al., 2017). In our system, A485 mildly but significantly increased the fraction of synthetic TFs bound to chromatin relative to control (Fig. 5A).

This result supports the possibility that TFs can be tethered to chromatin through protein-protein interactions with p300.

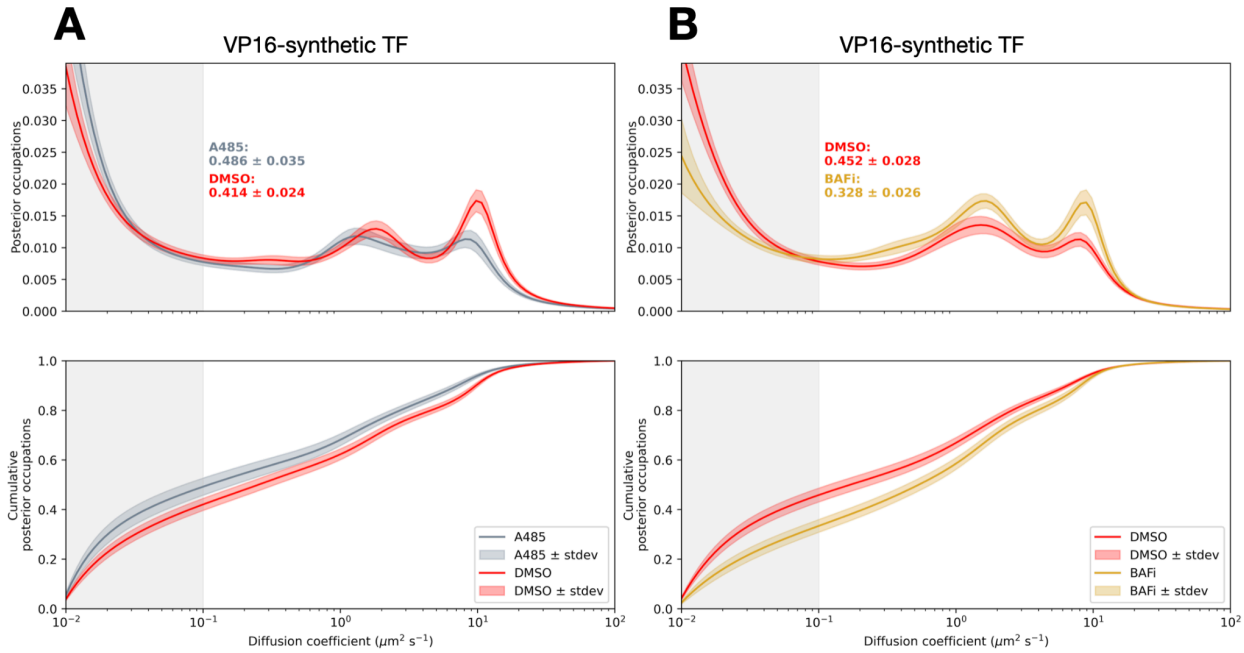

Figure 5: Perturbing coactivator function alters TF bound fraction
A: VP16-synthetic transcription factor diffusion spectra for cells treated for two hours with BAFi or vehicle (DMSO).
B: VP16-synthetic transcription factor diffusion spectra for cells treated for two hours with A485 or vehicle (DMSO).

As a second perturbation of coactivator function, we inhibited the BAF (mammalian Swi/Snf) complex with BAFi (BRM014). BAF inhibition leads to rapid genome-wide chromatin compaction and decreased global transcription (Schick et al., 2021). Recent single-molecule footprinting (SMF) experiments revealed that strong acidic activation domains enhance TF occupancy on DNA at a reporter locus (Doughty et al., 2024). This assay directly measures TF-DNA binding and showed that TFs with the strong VP48 activation domain exhibited greater occupancy compared to those with the DBD alone. Inhibiting BAF decreased promoter occupancy of the VP48 TF. We tested the effects of BAF inhibition on the chromatin binding of our synthetic TF (Fig. 5B). Inhibition of BAF significantly decreased the fraction of molecules bound to chromatin relative to the vehicle control. This result suggests that a substantial portion of our chromatin-bound TFs are at open or actively-transcribing loci.

Discussion

According to the traditional dogma on TF function, binding the genome should be controlled solely by the DBD and not be influenced by IDRs, much less by short activation domains. We broke this expectation by demonstrating that short activation domains can control the fraction of TF molecules bound to chromatin. Mutations that increase activation domain strength in reporter assays increase the fraction of molecules bound to chromatin. Conversely, mutations that decrease activation domain strength decrease the fraction of molecules bound to chromatin. This trend holds for three structurally diverse DBDs and for both synthetic and full length TFs. Our result adds to the accumulating cracks in the standard model (Chen et al., 2022; Sun et al., 2021).

SMT has revealed many new dimensions of TF nuclear dynamics and has been instrumental for our discovery. The technique has shown that TF-chromatin interactions are short lived (Brouwer and Lenstra, 2019; Lionnet and Wu, 2021, 2021; Liu et al., 2014) and that IDRs can make larger contributions to chromatin binding than DBDs (Chen et al., 2022). Here we add that minimal activation domains can control the fraction of molecules bound to chromatin.

There are three hypotheses for how increasing activation domain strength led to a higher fraction of TF molecules bound to chromatin: (1) activation domains could directly bind DNA, (2) activation domains could modulate DBD interactions with DNA, or (3) activation domains could bind to other proteins (i.e. coactivators) that are bound to chromatin, tethering the TF to chromatin.

It is unlikely that our short acidic activation domains directly bind to DNA because of electrostatic repulsion. All of our acidic activation domains are negatively charged and repel negatively charged DNA. While protein net charge can play a large role in nuclear diffusion (Xiang et al., 2020), we found no correlation between net charge and fractions bound in factors we tested (Fig. S7).

It is possible our activation domains are interacting with the DBD to modulate DNA binding. There are emerging examples of how intramolecular activation domain-DBD interactions can increase the DNA binding specificity of the TF. In p53, electrostatic interactions between the activation domain and DBD outcompete random DNA and increase specificity (He et al., 2019; Krois et al., 2018; Sun et al., 2021). The proline-rich region of RelA increases affinity for random DNA (Baughman et al., 2022). In Sox2, the activation domain and DBD interact in solution and disengage upon DNA

binding (Bjarnason et al., 2024). For our results, we believe intramolecular interactions are not the main drivers of chromatin binding because the phenotype is consistent across three structurally distinct DBDs. As a result, we do not favor the hypothesis that our phenomenon is due to interactions between the activation domain and the DBD.

We favor the hypothesis that protein-protein interactions between activation domains and coactivators explain the observed relationship between activation domain strength and the fraction of molecules bound to chromatin. Coactivators bind to chromatin with longer dwell times than typical TFs, often contain many activation domain binding surfaces, and cluster at active loci (Cho et al., 2018; Dyson and Wright, 2016; Ferrie et al., 2024). Chromatin-bound coactivators could tether TFs to active loci. Mutations that increase affinity for coactivators would increase dwell times on chromatin, increasing the bound fraction. In yeast, targeting the Med15 coactivator subunit to a new locus is sufficient to recruit the Msn2 TF (Mindel et al., 2024b). Our two pharmacological perturbations of coactivator function, while not conclusive, are consistent with this hypothesis. Unraveling the molecular mechanism for how strong activation domains increase chromatin binding is an exciting future direction.

We anticipate that only some activation domains will tether TFs to chromatin. Different classes of activation domains bind distinct coactivators, and we suspect that only some of these interactions will be strong enough to tether TFs to chromatin. Promising avenues for further investigation include more targeted pharmacology to disrupt specific activation domain coactivator interactions or proximity-assisted photoactivation (Graham et al., 2022).

We cannot yet distinguish whether these short activation domains increase DNA binding or chromatin binding. In this study, we measured chromatin binding of TFs in aggregate. While we can see single molecules diffusing in the nucleus, we could neither visualize the reporter locus nor identify which genomic sites these TFs occupied. We have no evidence that activation-domain-mediated chromatin binding confers any DNA sequence specificity or genomic localization. Indeed, most of our binding must be at loci without a cognate motif because the DBD has been engineered to have no exact motif matches in the human genome. Consequently, we believe that activation-domain-mediated chromatin binding is a phenomenon distinct from the ability of long IDRs to direct TFs to specific genomic loci (Brodsky et al., 2020; Gera et al., 2022; Goldman et al., 2023). Conversely, we believe that the same underlying biological process gives rise to our SMT results and others' SMF results that show that activation domains enhance promoter occupancy (Doughty et al., 2024).

We speculate that activation domains can reinforce DBD binding to clusters of cognate motifs. There is clear evidence that DBDs contribute to both DNA binding and chromatin binding (Brodsky et al., 2020; Chen et al., 2022; Liu et al., 2014). Activation domains cannot substitute for DBDs. SMF assays (Doughty et al., 2024) support a feedforward mechanism for binding motif clusters: the DBD binds one motif and the activation domain recruits chromatin remodelers that evict nucleosomes, revealing additional motifs for DBD binding. Multivalency and avidity increase local concentration. The DBD still confers genome specificity, and the activation domain merely reinforces binding at binding site clusters, which are enriched in enhancers. Both the activation domain and DBD are necessary and mutually reinforcing for selecting target sites (Staller et al., 2022).

Our results also challenge the traditional interpretation of activation domain strength. Previously, we had assumed that all our synthetic TFs had similar DNA occupancy because they have the same DBD. Our results here show that strong activation domains increase chromatin binding. As a result, the observed changes in reporter activity are a convolution of more binding and more coactivator recruitment, which cannot be easily deconvolved. This finding motivates the need for new assays for activation domain function that can separate binding from reporter activity.

In this work, we focused on the fraction of molecules bound to chromatin. We also see some changes in the distribution of inferred diffusion constants of mobile molecules, some of which are bimodal. We speculate that the slow-moving population might be TFs bound to partners exploring the nucleus as clusters or “wolf packs,” as we hypothesized (Staller 2022). Testing this intriguing idea will require emerging methods, like proximity-assisted photoactivation (Graham et al., 2022).

Materials and methods

U2OS cell culture and transfection

U2OS cells (osteosarcoma from a 15-year-old female) were maintained at 37°C in a humidified atmosphere with 5% CO_2. Cells were cultured in reconstituted DMEM containing 4.5 g/L glucose (Thermo 12800082) supplemented with 9% fetal bovine serum (“FBS”, HyClone), L-glutamine (Sigma), GlutaMax (Thermo), and 100 U/mL penicillin-streptomycin (Thermo). Cells were generally passaged every three days by splitting 1:8, using 0.25% trypsin to facilitate detachment.

Cell lines used in this study tested negative for mycoplasma about monthly by PCR (https://bitesizebio.com/23682/homemade-pcr-test-for-mycoplasma-contamination/).

For imaging constructs expressed off plasmids, U2OS cells were electroporated using a homemade buffer (dx.doi.org/10.17504/protocols.io.64mhgu6) and the X-001 protocol of the Lonza Nucleofector II. This method mitigates autofluorescence artifacts from lipid-based transfection reagents.

For generation of cell lines, U2OS cells were transfected in 6-well dishes using Lipofectamine™ 3000, with 3 µg of DNA and 6 µL of Lipofectamine™ 3000 per well.

U2OS cell line generation

To generate the reporter cell line, U2OS cells were transfected with a combined 1 µg of Cas9 and sgRNA plasmid targeting the AAVS1 locus, as well as 2 µg of repair template containing the reporter locus, similar to that of the previously-described construct (Staller et al., 2022). The reporter construct is based on a published reporter (Addgene #176294), but we replaced puromycin resistance with blasticidin resistance, added VKYY to the start of the GFP to boost translation (Verma et al., 2019), inserted a small t intron, and inserted a WPRE before the SV40 poly(A) signal.

Two days after transfection, cells were passaged onto a 10 cm dish and selected with blasticidin (Fischer A1113903) at 5 µg/mL. When this dish was confluent, single clones were isolated by limiting dilution into 96-well plates and sequence-validated to have at least one copy of the reporter locus by PCR and Sanger sequencing. Clones were also tested by transient transfection of a VP16 synthetic TF by measuring fold-induction in response to estradiol induction. We picked the most robustly induced clone for this study. Cells were maintained in media containing 5 µg/mL blasticidin.

All synthetic zinc-finger- and SOX2DBD-bearing constructs were cloned using Gibson Assembly and verified via whole-plasmid sequencing (Plasmidsaurus). Starting with a published synthetic TF (Addgene #176293), we moved the TF into PiggyBac backbone with a L30 promoter, replaced mScarlet with HaloTag, added an V5 tag, and replaced the neomycin resistance with puromycin resistance. These constructs were stably integrated into the reporter clone described above. For integrations, we transfected 2 µg of a synthetic construct with 1 µg of a vector expressing Super PiggyBac Transposase (Yusa et al., 2011) in this reporter clone. Two days after transfection, we passaged cells onto a 10 cm dish and selected cells with puromycin (Invivogen) at 1 µg/mL. We continued passaging these cells for at least two weeks

before proceeding with experiments. Cells were maintained in media containing 5 μL/mL blasticidin and 1 μg/mL puromycin.

Drug treatments and nucleofection

For Fig. 5B, uninduced cells were treated for 2 hours with 10 μM BRM/BRG1 ATP Inhibitor-1 compound 14 (MedChemExpress; “BAFi”) or the equivalent DMSO. These cells were stained with HaloTag ligand (as in “Sample preparation for imaging experiments”) and induced with 1 μM β-Estradiol (Sigma E2758; “estradiol”) immediately before imaging.

For Fig. 5A, uninduced cells were treated for 2 hours with 10 μM A485 (Fischer) or the equivalent DMSO. These cells were stained with HaloTag ligand (as in “Sample preparation for imaging experiments”) and induced with 1 μM estradiol immediately before imaging.

For Figs. 4B and C, 1 million U2OS cells were electroporated with previously-described constructs (Chen et al., 2022) and treated with deferoxamine mesylate salt (Sigma D9533, “DFO”) at 100 μM overnight.

Except treatments noted above in this section, cells in all other conditions were treated with 1 μM estradiol for 12-16 hours the night before they were imaged for SMT.

For all flow cytometry experiments, cells were treated with 1 μM estradiol for 28 hours.

Sample preparation for imaging experiments

For imaging experiments, cells were plated the evening prior to imaging to achieve 60–80% confluency on the day of imaging. Cells were grown on glass-bottom dishes (MatTek P35G-1.5-14-C) in phenol-red-free DMEM containing 4.5 g/L glucose and supplemented with 9% FBS and 100 U/mL penicillin-streptomycin ("imaging medium").

Cells were stained for SMT as follows: the day of imaging, cells were stained for 5 minutes with JFX650-HaloTag ligand (generously gifted by the Lavis lab) added to a final concentration of 5 nM and 2 μM Hoechst 33342 (Thermo), rinsed once with imaging medium, and incubated in imaging medium for 10 minutes. The dishes were rinsed one more time, replenished with imaging medium, and mounted on the microscope with Nikon immersion oil Type F.

Cells were stained for FRAP as follows: the day of imaging, cells were stained for 5 minutes with TMR-HaloTag ligand (Promega) added to a final concentration of 50 nM, rinsed once with imaging medium, and incubated in imaging medium for 10 minutes. The dishes were rinsed one more time, replenished with imaging medium, and mounted on the microscope with Immersol 518 F (Zeiss). The dish was then left to equilibrate thermally for about 5 minutes prior to imaging.

Flow cytometry and sample preparation

The day of the assay, cells were stained for 10 minutes with 35 nM of JFX650-HaloTag ligand and 10 μM Hoechst 33342 (Thermo), rinsed once with imaging medium, and incubated in imaging medium for 25 minutes. Cells were lifted using 0.25% trypsin, quenched with imaging medium, and filtered through a cell strainer to remove clumps.

Flow cytometry was conducted on a BD Bioscience LSR Fortessa in the UC Berkeley Flow Cytometry Core. Conditions presented together as panels were collected on the same day with the same voltages. However, these voltages were not always kept consistent from day to day, as daily CST calibration often changed cytometer baselines.

Data were analyzed using FlowJo, with consistent gating applied across conditions that are presented together in a panel. The reporter fluorescence distributions were frequently bimodal, so we quantified reporter activity in two ways. First, we used the fraction of cells that were GFP positive, but this metric had a limited dynamic range. Second, we used the mean fluorescence intensity (MFI) of GFP-positive (GFP+) cells, which had a larger dynamic range.

SMT movie acquisition

The microscope used for SMT is as previously described (Hansen et al., 2017). In brief, this imaging setup consisted of a Nikon TI microscope fitted with a 100X/NA 1.49 oil-immersion TIRF objective, a motorized mirror, a Perfect Focus system, an EM-CCD camera, and an incubation chamber maintained at 37°C with a humidified 5% CO_2 atmosphere. The laser launch includes lasers of the following wavelengths: 405 nm (140 mW, OBIS, Coherent), 488 nm, 561 nm, and 639 nm (all 1 W, Genesis, Coherent). Laser intensities were regulated using an acousto-optic tunable filter (AA Opto-Electronic, AOTFnC-VIS-TN) and triggered via the camera's TTL exposure output signal. Lasers were delivered to the microscope through an optical fiber, reflected by a

quad-band dichroic mirror (405 nm/488 nm/561 nm/633 nm, Semrock), and focused at the back focal plane of the objective. The incident laser angle was adjusted to achieve highly inclined laminated optical sheet (HILO) illumination (Tokunaga et al., 2008). Emission light was filtered using the appropriate Semrock single band-pass filters.

For the diffusion spectra shown in each panel, all conditions were imaged on the same day to minimize day-to-day variability. A second replicate was imaged on a different day, and the data from both days were pooled to generate the reported spectra.

All experiments except those in Figs. 4B, C and S3 used the automated imaging scheme previously described (Walther et al., 2024). Briefly, custom NIS Elements Macro Language and Python scripts instructed the microscope to raster over a coverslip, taking 81.92 µm x 81.92 µm images at each grid point. Cell presence in a field was determined using StarDist segmentation (Schmidt et al., 2018) in the Hoescht channel; images in additional channels of interest (GFP: 488 nm, JFX650: 639 nm) were also acquired. If cells were identified, one was randomly selected for imaging at 7.48 ms using the following protocol: 1200 frames with 2 ms stroboscopic illumination of the 639 nm laser (1 W, 100%), followed by 1200 frames with 2 ms stroboscopic illumination of the 639 nm laser (1 W, 100%) combined with 30% 405 nm laser power during camera transition intervals, and finally 1200 frames with 2 ms stroboscopic illumination of the 639 nm laser (1 W, 100%) combined with 60% 405 nm laser power during camera transition intervals. The 405 nm laser pulses during transition times were used to reactivate dark JFX650 fluorophores (Endesfelder and Heilemann, 2015) while minimizing background contribution by the laser pulse itself.

SMT analysis

Spots were detected, subpixel-localized, and linked into trajectories using algorithms within the open-source Python package quot (https://github.com/alecheckert/quot): 'filter': {'start': 0, 'method': 'identity'}, 'detect': {'method': 'llr', 'k': 1.5, 'w': 11, 't': 18.0}, 'localize': {'method': 'ls_int_gaussian', 'window_size': 11, 'sigma': 1.5, 'ridge': 0.0001, 'max_iter': 10, 'damp': 0.3, 'camera_gain': 109.0, 'camera_bg': 470.0}, 'track': {'method': 'conservative', 'pixel_size_um': 0.16, 'search_radius': 1.0, 'max_blinks': 0, 'min_I0': 0.0}. Frames with more than 6 localizations in nuclei were not tracked.

We segmented Hoescht-stained cell nuclei images with either StarDist (Schmidt et al., 2018) or cellpose (Stringer et al., 2021) as a starting point but found that manual

QC and refining were necessary for accurate masking. This was done with a custom Python GUI (https://github.com/vinsfan368/qtpicker). We only analyze trajectories whose points lie entirely within one, and only one, of these curated masks.

The resulting masked trajectories were analyzed using the open-source and previously-published Python package saspt (https://github.com/alecheckert/saspt; Heckert et al., 2022). We used the following inference parameters: focal_depth=0.7, sample_size=1000000, likelihood_type='rbme', splitsize=3, start_frame=0 (with the sample_size parameter being arbitrarily large to analyze all trajectories). For Figs. 4B and C, we used the above parameters but replaced splitsize=3 with splitsize=8 to maintain consistency with our previously-published results (Chen et al., 2022).

In figures where errors are reported, we followed a similar scheme previously described in (Ferrie et al., 2024): for a dataset comprising n cells, we subsampled n random cells with replacement 96 times. For each of these trials, we pooled all trajectories from the n random cells, ran inference using the parameters described above, and noted the fractions bound. The bootstrapping means, standard deviations, and 95% confidence intervals are reported and/or plotted where indicated.

To quantitatively describe sources of variance (Fig. S2) within our data in a non-model-dependent and computationally-cheap way, we were inspired by (Driouchi et al., 2023). Briefly, we collate trajectories, noting the day on which they were imaged and the cell from which they were collected. We then decompose this data into individual displacements and subsample arbitrary numbers (n) of these jumps 1000 times, noting the mean value of these 1000 trials. By varying both n and the sampling scheme, we can assess sources of variance. We sampled according to three schemes: (1, gray) n jumps from the entire pool of trajectories, which establishes the baseline and should follow the law of large numbers as n becomes larger; (2, blue) by picking one cell from the dataset and sampling n jumps from only that cell; and (3, orange) by picking an imaging day from the dataset and sampling n jumps only imaged on that day. When curves 2 and 3 diverge from 1, all variance with respect to n has been captured. We note that variability between fields-of-view could contribute to cell-to-cell variability, but given that most of our fields-of-view contained only one cell, we did not quantify this source of variability. We found in Fig. S2 that cell-to-cell variability is about 100x higher than day-to-day variability.

FRAP movie acquisition

FRAP was conducted using a ZEISS LSM900 Airyscan 2 laser-scanning confocal microscope mounted on an inverted Axio Observer.Z1/7 platform and operated with ZEN 3.1 blue software. The system was equipped with a temperature- and CO_2-controlled incubation chamber (Zeiss/PeCon) maintained at 37°C and 5% CO_2. Fluorophores were excited using a 561 nm laser with a maximally-sized pinhole, 3.5% laser power, and 800 V detector gain. Movies were acquired with bidirectional scanning and 8-bit depth to maximize scan speeds. Photobleaching (100% 561 nm laser and 100% 405 nm laser) was applied during frame 21, and the first 20 frames were used to normalize the fractional recovery to start at 1.

FRAP analysis

We used custom Python code (https://github.com/vinsfan368/FRAPanalysis) to quality-control FRAP movies and calculate normalized recoveries. FRAP movies were rejected if there was substantial axial drift. A max-intensity projection of each FRAP movie was made and blurred to generate a nuclear mask for the movie. The initial FRAP spot was recovered from CZI file metadata and drift-corrected using 2D image cross-correlation. We defined FRAP recovery at a given time point as:

$$I_{spot}(t) - bg(t) \,/\, I_{nuc}(t) - bg(t) \qquad (1)$$

where I_{spot} is mean intensity within the bleach spot, I_{nuc} is the mean intensity of the nuclear mask (which includes the bleach spot), and bg is an estimate of image background, the median pixel intensity of pixels outside of the nuclear mask. We then defined normalized FRAP recovery at a given time point by dividing (1) by:

$$(I_{spot}(t_{1\text{-}20}) - bg(t_{1\text{-}20})) \,/\, (I_{nuc}(t_{1\text{-}20}) - bg(t_{1\text{-}20}))$$

where $t_{1\text{-}20}$ is the average value of the pre-bleach frames. Complete FRAP recovery would reach a normalized value of 1.

Our FRAP recoveries were poorly described by single-exponential equations (with the exception of H2B); we fit them to a double-exponential equation with a constant term:

$$(A_1 * (1 - \exp(dt/\text{-}tau_1))) + (A_2 * (1 - \exp(dt/\text{-}tau_2))) + C$$

constraining A_1, A_2, and C to [0, 1] and $A_1 + A_2 + C$ to 1. Because fitting FRAP recovery curves carries model-dependent assumptions (Sprague et al., 2004) and can be numerically unstable, we choose not to report residence time values from these fits.

Acknowledgements

A heartfelt thank you to all members of the Tjian+Darzacq and Staller groups for their intellectual input and experimental advice for this project, particularly Djem Kissiov, Claudia Cattoglio, Joseph McKenna, Yu Chen, Aditya Udupa, and Abrar Abidi. A large thanks goes to Thomas Graham and Sathvik Anantakrishnan for their efforts on microscope automation and maintenance, without which this project would not have been possible. We thank Djem Kissiov, Aditya Udupa, and Robert Tjian for the careful reading of the manuscript, which led to its substantial improvement. We thank Anders Näär and Haribabu Arthanari for helpful discussions. We thank Luke Lavis for providing us with Janelia Fluor dyes.

Author contributions

V.B.F. and M.V.S. conceptualized the study. V.B.F. executed experiments and performed analysis. M.V.S. and X.D. supervised the project. V.B.F. and M.V.S. wrote the manuscript. X.D. revised the manuscript and funded the project.

Funding

M.V.S. is supported by Simons Foundation grant 1018719, NSF grant 2112057, and NIH grant R35GM150813. M.V.S. is a Chan Zuckerberg Biohub – San Francisco Investigator. Funding to X.D. was provided by the Silicon Valley Community Foundation/CZI (RR-8175).

Competing interests

X.D. is a co-founder of Eikon Therapeutics, Inc.

References

Alerasool, N., Leng, H., Lin, Z.-Y., Gingras, A.-C., Taipale, M., 2022. Identification and functional characterization of transcriptional activators in human cells. Mol. Cell 82, 677-695.e7. https://doi.org/10.1016/j.molcel.2021.12.008

Baughman, H.E.R., Narang, D., Chen, W., Villagrán Suárez, A.C., Lee, J., Bachochin, M.J., Gunther, T.R., Wolynes, P.G., Komives, E.A., 2022. An intrinsically disordered transcription activation domain increases the DNA binding affinity and reduces the specificity of NFκB p50/RelA. J. Biol. Chem. 298, 102349. https://doi.org/10.1016/j.jbc.2022.102349

Bjarnason, S., McIvor, J.A.P., Prestel, A., Demény, K.S., Bullerjahn, J.T., Kragelund,

B.B., Mercadante, D., Heidarsson, P.O., 2024. DNA binding redistributes activation domain ensemble and accessibility in pioneer factor Sox2. Nat. Commun. 15, 1445. https://doi.org/10.1038/s41467-024-45847-2
Brent, R., Ptashne, M., 1985. A eukaryotic transcriptional activator bearing the DNA specificity of a prokaryotic repressor. Cell 43, 729–736. https://doi.org/10.1016/0092-8674(85)90246-6
Brodaczewska, K.K., Szczylik, C., Fiedorowicz, M., Porta, C., Czarnecka, A.M., 2016. Choosing the right cell line for renal cell cancer research. Mol. Cancer 15, 83. https://doi.org/10.1186/s12943-016-0565-8
Brodsky, S., Jana, T., Mittelman, K., Chapal, M., Kumar, D.K., Carmi, M., Barkai, N., 2020. Intrinsically Disordered Regions Direct Transcription Factor In Vivo Binding Specificity. Mol. Cell 79, 459-471.e4. https://doi.org/10.1016/j.molcel.2020.05.032
Brouwer, I., Lenstra, T.L., 2019. Visualizing transcription: key to understanding gene expression dynamics. Curr. Opin. Chem. Biol., Chemical Genetics and Epigenetics • Molecular Imaging 51, 122–129. https://doi.org/10.1016/j.cbpa.2019.05.031
Chen, Y., Cattoglio, C., Dailey, G.M., Zhu, Q., Tjian, R., Darzacq, X., 2022. Mechanisms governing target search and binding dynamics of hypoxia-inducible factors. eLife 11, e75064. https://doi.org/10.7554/eLife.75064
Cho, W.-K., Spille, J.-H., Hecht, M., Lee, C., Li, C., Grube, V., Cisse, I.I., 2018. Mediator and RNA polymerase II clusters associate in transcription-dependent condensates. Science 361, 412–415. https://doi.org/10.1126/science.aar4199
Cress, A., Triezenberg, S.J., 1991. Nucleotide and deduced amino acid sequences of the gene encoding virion protein 16 of herpes simplex virus type 2. Gene 103, 235–238. https://doi.org/10.1016/0378-1119(91)90278-j
DelRosso, N., Suzuki, P.H., Griffith, D., Lotthammer, J.M., Novak, B., Kocalar, S., Sheth, M.U., Holehouse, A.S., Bintu, L., Fordyce, P., 2024. High-throughput affinity measurements of direct interactions between activation domains and co-activators. https://doi.org/10.1101/2024.08.19.608698
DelRosso, N., Tycko, J., Suzuki, P., Andrews, C., Aradhana, Mukund, A., Liongson, I., Ludwig, C., Spees, K., Fordyce, P., Bassik, M.C., Bintu, L., 2023. Large-scale mapping and mutagenesis of human transcriptional effector domains. Nature 616, 365–372. https://doi.org/10.1038/s41586-023-05906-y
Doughty, B.R., Hinks, M.M., Schaepe, J.M., Marinov, G.K., Thurm, A.R., Rios-Martinez, C., Parks, B.E., Tan, Y., Marklund, E., Dubocanin, D., Bintu, L., Greenleaf, W.J., 2024. Single-molecule states link transcription factor binding to gene expression. Nature 1–10. https://doi.org/10.1038/s41586-024-08219-w
Driouchi, A., Bretan, M., Davis, B.J., Heckert, A., Seeger, M., Silva, M.B., Forrest, W.S., Hsiung, J., Tan, J., Yang, H., McSwiggen, D.T., Song, L., Sule, A., Abaie, B., Conroy, B., Elliott, L.A., Gonzalez, E., Ilkov, F., Isaacs, J., Labaria, G., Lagana, M., Larsen, D.D., Margolin, B., Nguyen, M.K., Rine, J., Tang, Y., Vana, M., Wilkey, A., Zhang, Z., Basham, S., Ho, J.J., Johnson, S., Klammer, A.A., Lin, K., Darzacq, X., Betzig, E., Berman, R.T., Anderson, D.J., 2023. Oblique Line Scan Illumination Enables Expansive, Accurate and Sensitive Single Protein Measurements in Solution and in Living Cells. https://doi.org/10.1101/2023.12.21.571765

Dyson, H.J., Wright, P.E., 2016. Role of Intrinsic Protein Disorder in the Function and Interactions of the Transcriptional Coactivators CREB-binding Protein (CBP) and p300*. J. Biol. Chem. 291, 6714–6722. https://doi.org/10.1074/jbc.R115.692020

El-Gebali, S., Mistry, J., Bateman, A., Eddy, S.R., Luciani, A., Potter, S.C., Qureshi, M., Richardson, L.J., Salazar, G.A., Smart, A., Sonnhammer, E.L.L., Hirsh, L., Paladin, L., Piovesan, D., Tosatto, S.C.E., Finn, R.D., 2019. The Pfam protein families database in 2019. Nucleic Acids Res. 47, D427–D432. https://doi.org/10.1093/nar/gky995

Endesfelder, U., Heilemann, M., 2015. Direct stochastic optical reconstruction microscopy (dSTORM). Methods Mol. Biol. Clifton NJ 1251, 263–276. https://doi.org/10.1007/978-1-4939-2080-8_14

Erijman, A., Kozlowski, L., Sohrabi-Jahromi, S., Fishburn, J., Warfield, L., Schreiber, J., Noble, W.S., Söding, J., Hahn, S., 2020. A High-Throughput Screen for Transcription Activation Domains Reveals Their Sequence Features and Permits Prediction by Deep Learning. Mol. Cell 78, 890-902.e6. https://doi.org/10.1016/j.molcel.2020.04.020

Ferrie, J.J., Karr, J.P., Graham, T.G.W., Dailey, G.M., Zhang, G., Tjian, R., Darzacq, X., 2024. p300 is an obligate integrator of combinatorial transcription factor inputs. Mol. Cell 84, 234-243.e4. https://doi.org/10.1016/j.molcel.2023.12.004

Finn, R.D., Coggill, P., Eberhardt, R.Y., Eddy, S.R., Mistry, J., Mitchell, A.L., Potter, S.C., Punta, M., Qureshi, M., Sangrador-Vegas, A., Salazar, G.A., Tate, J., Bateman, A., 2016. The Pfam protein families database: towards a more sustainable future. Nucleic Acids Res. 44, D279-285. https://doi.org/10.1093/nar/gkv1344

Gera, T., Jonas, F., More, R., Barkai, N., 2022. Evolution of binding preferences among whole-genome duplicated transcription factors. eLife 11, e73225. https://doi.org/10.7554/eLife.73225

Gill, G., Pascal, E., Tseng, Z.H., Tjian, R., 1994. A glutamine-rich hydrophobic patch in transcription factor Sp1 contacts the dTAFII110 component of the Drosophila TFIID complex and mediates transcriptional activation. Proc. Natl. Acad. Sci. U. S. A. 91, 192–196.

Gillespie, M.A., Palii, C.G., Sanchez-Taltavull, D., Shannon, P., Longabaugh, W.J.R., Downes, D.J., Sivaraman, K., Espinoza, H.M., Hughes, J.R., Price, N.D., Perkins, T.J., Ranish, J.A., Brand, M., 2020. Absolute Quantification of Transcription Factors Reveals Principles of Gene Regulation in Erythropoiesis. Mol. Cell 78, 960-974.e11. https://doi.org/10.1016/j.molcel.2020.03.031

Goldman, N., Chandra, A., Johnson, I., Sullivan, M.A., Patil, A.R., Vanderbeck, A., Jay, A., Zhou, Y., Ferrari, E.K., Mayne, L., Aguilan, J., Xue, H.-H., Faryabi, R.B., Wherry, E.J., Sidoli, S., Maillard, I., Vahedi, G., 2023. Intrinsically disordered domain of transcription factor TCF-1 is required for T cell developmental fidelity. Nat. Immunol. 24, 1698–1710. https://doi.org/10.1038/s41590-023-01599-7

Graham, T.G., Ferrie, J.J., Dailey, G.M., Tjian, R., Darzacq, X., 2022. Detecting molecular interactions in live-cell single-molecule imaging with proximity-assisted photoactivation (PAPA). eLife 11, e76870. https://doi.org/10.7554/eLife.76870

Grimm, J.B., Xie, L., Casler, J.C., Patel, R., Tkachuk, A.N., Falco, N., Choi, H., Lippincott-Schwartz, J., Brown, T.A., Glick, B.S., Liu, Z., Lavis, L.D., 2021. A General Method to Improve Fluorophores Using Deuterated Auxochromes. JACS

Au 1, 690–696. https://doi.org/10.1021/jacsau.1c00006
Guo, M., Song, L.-P., Jiang, Y., Liu, W., Yu, Y., Chen, G.-Q., 2006. Hypoxia-mimetic agents desferrioxamine and cobalt chloride induce leukemic cell apoptosis through different hypoxia-inducible factor-1α independent mechanisms. Apoptosis 11, 67–77. https://doi.org/10.1007/s10495-005-3085-3
Hansen, A.S., Pustova, I., Cattoglio, C., Tjian, R., Darzacq, X., 2017. CTCF and cohesin regulate chromatin loop stability with distinct dynamics. eLife 6, e25776. https://doi.org/10.7554/eLife.25776
Hansen, A.S., Woringer, M., Grimm, J.B., Lavis, L.D., Tjian, R., Darzacq, X., 2018. Robust model-based analysis of single-particle tracking experiments with Spot-On. eLife 7, e33125. https://doi.org/10.7554/eLife.33125
He, F., Borcherds, W., Song, T., Wei, X., Das, M., Chen, L., Daughdrill, G.W., Chen, J., 2019. Interaction between p53 N terminus and core domain regulates specific and nonspecific DNA binding. Proc. Natl. Acad. Sci. 116, 8859–8868. https://doi.org/10.1073/pnas.1903077116
Heckert, A., Dahal, L., Tjian, R., Darzacq, X., 2022. Recovering mixtures of fast-diffusing states from short single-particle trajectories. eLife 11, e70169. https://doi.org/10.7554/eLife.70169
Henderson, A.R., Henley, M.J., Foster, N.J., Peiffer, A.L., Beyersdorf, M.S., Stanford, K.D., Sturlis, S.M., Linhares, B.M., Hill, Z.B., Wells, J.A., Cierpicki, T., Brooks, C.L., Fierke, C.A., Mapp, A.K., 2018. Conservation of coactivator engagement mechanism enables small-molecule allosteric modulators. Proc. Natl. Acad. Sci. 115, 8960–8965. https://doi.org/10.1073/pnas.1806202115
Kotha, S.R., Staller, M.V., 2023. Clusters of acidic and hydrophobic residues can predict acidic transcriptional activation domains from protein sequence. Genetics 225, iyad131. https://doi.org/10.1093/genetics/iyad131
Krois, A.S., Dyson, H.J., Wright, P.E., 2018. Long-range regulation of p53 DNA binding by its intrinsically disordered N-terminal transactivation domain. Proc. Natl. Acad. Sci. 115, E11302–E11310. https://doi.org/10.1073/pnas.1814051115
Lasko, L.M., Jakob, C.G., Edalji, R.P., Qiu, W., Montgomery, D., Digiammarino, E.L., Hansen, T.M., Risi, R.M., Frey, R., Manaves, V., Shaw, B., Algire, M., Hessler, P., Lam, L.T., Uziel, T., Faivre, E., Ferguson, D., Buchanan, F.G., Martin, R.L., Torrent, M., Chiang, G.G., Karukurichi, K., Langston, J.W., Weinert, B.T., Choudhary, C., de Vries, P., Van Drie, J.H., McElligott, D., Kesicki, E., Marmorstein, R., Sun, C., Cole, P.A., Rosenberg, S.H., Michaelides, M.R., Lai, A., Bromberg, K.D., 2017. Discovery of a potent catalytic p300/CBP inhibitor that targets lineage-specific tumors. Nature 550, 128–132. https://doi.org/10.1038/nature24028
Lionnet, T., Wu, C., 2021. Single-molecule tracking of transcription protein dynamics in living cells: seeing is believing, but what are we seeing? Curr. Opin. Genet. Dev., Genome Architecture and Expression 67, 94–102. https://doi.org/10.1016/j.gde.2020.12.001
Liu, Z., Legant, W.R., Chen, B.-C., Li, L., Grimm, J.B., Lavis, L.D., Betzig, E., Tjian, R., 2014. 3D imaging of Sox2 enhancer clusters in embryonic stem cells. eLife 3, e04236. https://doi.org/10.7554/eLife.04236
Mindel, V., Brodsky, S., Cohen, A., Manadre, W., Jonas, F., Carmi, M., Barkai, N.,

2024a. Intrinsically disordered regions of the Msn2 transcription factor encode multiple functions using interwoven sequence grammars. Nucleic Acids Res. 52, 2260–2272. https://doi.org/10.1093/nar/gkad1191

Mindel, V., Brodsky, S., Yung, H., Manadre, W., Barkai, N., 2024b. Revisiting the model for coactivator recruitment: Med15 can select its target sites independent of promoter-bound transcription factors. Nucleic Acids Res. 52, 12093–12111. https://doi.org/10.1093/nar/gkae718

Morffy, N., Van den Broeck, L., Miller, C., Emenecker, R.J., Bryant, J.A., Lee, T.M., Sageman-Furnas, K., Wilkinson, E.G., Pathak, S., Kotha, S.R., Lam, A., Mahatma, S., Pande, V., Waoo, A., Wright, R.C., Holehouse, A.S., Staller, M.V., Sozzani, R., Strader, L.C., 2024. Identification of plant transcriptional activation domains. Nature 632, 166–173. https://doi.org/10.1038/s41586-024-07707-3

Ning, S., Chao, H.-J., Li, S., Zhou, R., Zou, L., Zhang, X., Liu, J., Yan, D., Duan, M., 2022. The auto-inhibition mechanism of transcription factor Ets-1 induced by phosphorylation on the intrinsically disordered region. Comput. Struct. Biotechnol. J. 20, 1132–1141. https://doi.org/10.1016/j.csbj.2022.02.025

Park, M., Patel, N., Keung, A.J., Khalil, A.S., 2019. Engineering Epigenetic Regulation Using Synthetic Read-Write Modules. Cell 176, 227-238.e20. https://doi.org/10.1016/j.cell.2018.11.002

Sanborn, A.L., Yeh, B.T., Feigerle, J.T., Hao, C.V., Townshend, R.J., Lieberman Aiden, E., Dror, R.O., Kornberg, R.D., 2021. Simple biochemical features underlie transcriptional activation domain diversity and dynamic, fuzzy binding to Mediator. eLife 10, e68068. https://doi.org/10.7554/eLife.68068

Schick, S., Grosche, S., Kohl, K.E., Drpic, D., Jaeger, M.G., Marella, N.C., Imrichova, H., Lin, J.-M.G., Hofstätter, G., Schuster, M., Rendeiro, A.F., Koren, A., Petronczki, M., Bock, C., Müller, A.C., Winter, G.E., Kubicek, S., 2021. Acute BAF perturbation causes immediate changes in chromatin accessibility. Nat. Genet. 53, 269–278. https://doi.org/10.1038/s41588-021-00777-3

Schmidt, U., Weigert, M., Broaddus, C., Myers, G., 2018. Cell Detection with Star-Convex Polygons, in: Frangi, A.F., Schnabel, J.A., Davatzikos, C., Alberola-López, C., Fichtinger, G. (Eds.), Medical Image Computing and Computer Assisted Intervention – MICCAI 2018. Springer International Publishing, Cham, pp. 265–273. https://doi.org/10.1007/978-3-030-00934-2_30

Sprague, B.L., Pego, R.L., Stavreva, D.A., McNally, J.G., 2004. Analysis of Binding Reactions by Fluorescence Recovery after Photobleaching. Biophys. J. 86, 3473–3495. https://doi.org/10.1529/biophysj.103.026765

Staller, M.V., Holehouse, A.S., Swain-Lenz, D., Das, R.K., Pappu, R.V., Cohen, B.A., 2018. A High-Throughput Mutational Scan of an Intrinsically Disordered Acidic Transcriptional Activation Domain. Cell Syst. 6, 444-455.e6. https://doi.org/10.1016/j.cels.2018.01.015

Staller, M.V., Ramirez, E., Kotha, S.R., Holehouse, A.S., Pappu, R.V., Cohen, B.A., 2022. Directed mutational scanning reveals a balance between acidic and hydrophobic residues in strong human activation domains. Cell Syst. 13, 334-345.e5. https://doi.org/10.1016/j.cels.2022.01.002

Stormo, G.D., 2013. Modeling the specificity of protein-DNA interactions. Quant. Biol. Beijing China 1, 115–130. https://doi.org/10.1007/s40484-013-0012-4

Stringer, C., Wang, T., Michaelos, M., Pachitariu, M., 2021. Cellpose: a generalist algorithm for cellular segmentation. Nat. Methods 18, 100–106. https://doi.org/10.1038/s41592-020-01018-x

Sun, X., Dyson, H.J., Wright, P.E., 2021. A phosphorylation-dependent switch in the disordered p53 transactivation domain regulates DNA binding. Proc. Natl. Acad. Sci. U. S. A. 118, e2021456118. https://doi.org/10.1073/pnas.2021456118

Tokunaga, M., Imamoto, N., Sakata-Sogawa, K., 2008. Highly inclined thin illumination enables clear single-molecule imaging in cells. Nat. Methods 5, 159–161. https://doi.org/10.1038/nmeth1171

Trojanowski, J., Frank, L., Rademacher, A., Mücke, N., Grigaitis, P., Rippe, K., 2022. Transcription activation is enhanced by multivalent interactions independent of phase separation. Mol. Cell 82, 1878-1893.e10. https://doi.org/10.1016/j.molcel.2022.04.017

Udupa, A., Kotha, S.R., Staller, M.V., 2024. Commonly asked questions about transcriptional activation domains. Curr. Opin. Struct. Biol. 84, 102732. https://doi.org/10.1016/j.sbi.2023.102732

Verma, M., Choi, J., Cottrell, K.A., Lavagnino, Z., Thomas, E.N., Pavlovic-Djuranovic, S., Szczesny, P., Piston, D.W., Zaher, H.S., Puglisi, J.D., Djuranovic, S., 2019. A short translational ramp determines the efficiency of protein synthesis. Nat. Commun. 10, 5774. https://doi.org/10.1038/s41467-019-13810-1

Walther, N., Anantakrishnan, S., Graham, T.G.W., Dailey, G.M., Tjian, R., Darzacq, X., 2024. Automated live-cell single-molecule tracking in enteroid monolayers reveals transcription factor dynamics probing lineage-determining function. Cell Rep. 43. https://doi.org/10.1016/j.celrep.2024.114914

Xiang, L., Chen, K., Yan, R., Li, W., Xu, K., 2020. Single-molecule displacement mapping unveils nanoscale heterogeneities in intracellular diffusivity. Nat. Methods 17, 524–530. https://doi.org/10.1038/s41592-020-0793-0

Yusa, K., Zhou, L., Li, M.A., Bradley, A., Craig, N.L., 2011. A hyperactive piggyBac transposase for mammalian applications. Proc. Natl. Acad. Sci. U. S. A. 108, 1531–1536. https://doi.org/10.1073/pnas.1008322108